Accuracy of strain measurement systems on a non-isotropic material and its uncertainty on finite element analysis

Baldassarre, Alessandro; Ocampo, Juan; Martinez, Marcias; Rans, Calvin

DOI
10.1177/0309324720924580

Publication date
2020

Document Version
Accepted author manuscript

Published in
Journal of Strain Analysis for Engineering Design

Citation (APA)
Baldassarre, A., Ocampo, J., Martinez, M., & Rans, C. (2020). Accuracy of strain measurement systems on a non-isotropic material and its uncertainty on finite element analysis. *Journal of Strain Analysis for Engineering Design*, *56*(2), 76-95. https://doi.org/10.1177/0309324720924580

Accuracy of Strain Measurement Systems on a Non-Isotropic Material and its Uncertainty on Finite Element Analysis

Alessandro Baldassarre[1,a], *Juan Ocampo*[2b] *Marcias Martinez*[1,c], *Calvin Rans*[3,d]

[1] Department of Mechanical and Aeronautical Engineering, Clarkson University, 8 Clarkson Ave, Potsdam, NY 13699

[2] Department of Mechanical Engineering, St. Mary's University, 1 Camino Santa Maria, San Antonio, Texas, 78228

[3] Faculty of Aerospace Engineering, Delft University of Technology, Building 62, Kluyverweg 1, 2629 HS Delft

[a] baldaa@clarkson.edu, [b] jocampo@stmarytx.edu, [c] mmartine@clarkson.edu, [d] C.D.Rans@tudelft.nl

Keywords: Strains Monitoring, CFRP composite, Strain Gauges, Distributed Sensing System, Digital Image Correlation, Statistical methods, B-basis, Finite Element Analysis

Abstract

The application of Strain Gauges (SG) as recommended by the ASTM standards provides accurate strain measurements in isotropic materials. However, their use in composite materials becomes more challenging due to their anisotropic nature. In this study, we hypothesized that the use of the Distributed Sensing System (DSS) and the 3D Digital Image Correlation (DIC), which can average strain along a line and surface, respectively, may account for strain variability in composite materials. This study shows an investigation on the mechanical properties of unidirectional, cross-ply, and angle-ply carbon-epoxy specimens using SG, DSS, and DIC. The Bhattacharyya distance method was used to provide a preliminary evaluation of the closeness of the three different measurement techniques while the B-basis statistical method was used to analyze the experimental data in order to obtain a more conservative and reliable material parameter compared to the conventional averaged value, recommended by ASTM standards. Finally, a Finite Element model was created in Ansys Workbench™ as a means of evaluating the implication of a single point SG measurement, versus a line or a surface strain measurement. The FEA investigation was performed at a laminae level using the measured experimental elastic modulus and at a lamina-lamina level in which the elastic modulus of the unidirectional case was used as input in all the laminate configurations. The former analysis showed good agreement between the FEA and all the strain measurement systems with an averaged percentage difference below 5%. The latter analysis showed a higher discrepancy in the measured percentage difference. A comparison between the FEA and the SG measurements showed an overall percentage difference between the range of 10% and 26%. DSS and DIC-3D measurements provided an overall percentage difference below 10% for all the specimen configurations with a maximum percentage difference recorded for the longitudinal angle-ply case of approximately 9%.

Introduction

During the past decades, the use of composite materials has increased exponentially due to their extraordinary properties such as high strength-to-weight ratio, fatigue and corrosion resistance, low thermal expansion coefficient, high-impact strength along with many other aspects that made these materials suitable for many industrial applications. Examples include the use of composites in the aeronautical and aerospace industry, marine and infrastructure industry, where structural components operate in harsh environment. The layup configuration of composite laminates strictly depends on their application. Therefore, each configuration has its own mechanical properties. Current ASTM standards for orthotropic or anisotropic material recommend the use of strain gauges for characterizing the mechanical behavior of these materials [1] [2] [3]. However, strain gauges measurement on a single point in heterogeneous materials may lead to an overestimation or underestimation of the mechanical properties

compared to other strain measurement techniques that can monitor a wider area, such as Distributed Sensing System (DSS) (average over a line) and Digital Image Correlation (DIC) (average over a surface). In addition, since the measured material properties are used as input in the Finite Element Analysis (FEA) model, the evaluation of these parameters becomes crucial for an accurate numerical analysis of more complex structure.

Many authors addressed the material property characterizations of composite materials through the use of strain gauges [4], [5], [6]. The consequence of small misalignments of strain gauges can produce unacceptably high errors in measurement when applied on anisotropic materials. In an overview paper by Ajovalasit [6], it was shown that even for a small 5° misalignment, errors in the measured strain levels could be as high as 38% in CFRP and GRP composite structure. The transverse sensitivity of the strain gauges can also lead to significant errors in measuring the Poisson's ratio and shear modulus of anisotropic materials as discussed by Baumann and Naumann [5]. Some of the strain gauge manufacturers raised the matter on the performance of the strain gauges for inhomogeneous materials [7] [8]. These concerns are based on several factors such as the low thermal conductivity of the polymers as well as the gauge length and pattern. The former generates a heat concentration within the gauge that produces an increment in resistance which translates into a higher strain measurement error. The latter depends upon the application. In fact, while strain measurement through larger gauges (gauge length and pattern width) offer a better representation of the inhomogeneous material and provides a higher heat dissipation, they also reduce the stability and the measurement range increasing the averaging error.

In contrast, only few authors have determined mechanical properties in composite materials by using optical fiber [9] [10] [11]. In addition, most of the study that can be found in the literature used Fiber Bragg Grating (FBG) embedded within the laminate during the manufacturing process. Tests performed on carbon-epoxy specimens showed that the embedding of the optical fiber (100 µm diameter) did not affect the mechanical properties of the composite, as demonstrated by Roberts and Davidson [9], while it created a stress concentration element around the fiber on the impact and fatigue tests, as shown by J.M.A. Silva et al. [10].

Authors have also made use of DIC for characterizing the in-plane mechanical properties of composite materials [12] [13] [14] [15]. The subset size, the step size, and the region of interest chosen for the DIC prior testing can provide a discrete variation in the measured mechanical properties, as investigated by Kashfuddoja et al. on unidirectional CRFP laminates [12]. A comparison with the analytical equations of the rule of mixture and Halpin-Tsai model also showed a variation of approximately 1% and 2% in measuring the longitudinal elastic modulus and the major Poisson's ratio, respectively, while approximately 23% and 53% for the in-plane shear modulus and the transverse modulus, respectively. In a paper by Ab Ghani and Mahmud [13], it was shown that the discrepancy between the DIC data and the Representative Volume

Element (RVE) method used in the FEA was approximately 3.8%, 4.21%, and 6.75% for the CFRP, GFRP, and hybrid composite, respectively.

Several studies can be found in literature where the statistical approach, such as the Weibull distribution, was used to describe the strength of composite materials [16] [17] [18]. Currently, a two-parameter Weibull distribution approach is employed for composite structural design [19], which is based on the empirical calculation of the Weibull modulus and the scale parameter. A statistical analysis was performed by Barbero et al. [20] on the uncertainty Weibull modulus estimation based on a three-parameter Weibull distribution which is only function of the sample size. In addition, the authors used the A-basis and B-basis to determine flexural strength of Hexcel AS4/350-61 laminates. The B-basis method was accepted by the Federal Aviation Administration (FAA), Department of Defense (DoD), and the National Aeronautics and Space Administration (NASA) to satisfy the material strength probability levels required by Federal Regulations for metallic materials, as certified by the Metallic Materials Properties Development and Standardization (MMPDS) Handbook [21]. A modification of the three-parameter Weibull distribution was used by Nilakantan et al. [22] to evaluate the strength degradation due to weaving process and length-scale effects for Kevlar KM2 yarns. However, in contrast very few studies considered the Bhattacharyya distance method to estimate the variation of strain measurements within inhomogeneous materials. The Bhattacharyya distance was applied by Choi and Lee [23] as feature extraction method for two-class problems and multi-class problems showing good agreement with the conventional extraction method. The method was successfully applied by Jolad et. al [24] to measure the distance between two monochromatic signals at different amplitude and frequency.

In this study a one-to-one comparison of a line measurement is compared to a 2D surface measurement of the coupon. As such, the aim of this manuscript is to compare the accuracy in computing the longitudinal and transverse Elastic modulus in orthotropic and anisotropic materials through the use of Strain Gauges, DSS, and DIC. A statistical analysis methodology based on the Bhattacharyya distance was performed to preliminary assess the discrepancy in strain measurements. In addition, a B-Basis statistical analysis was performed in order to choose a conservative and reliable value of Elastic Modulus in unidirectional specimens. As statistical method, the B-basis was applied to measurements obtained on carbon fiber epoxy specimens evaluated in this study, and evaluated to determine how the measured mechanical parameters compares when applied to cross-ply and angle ply configurations in a FE model. Finally, Finite Element Analysis (FEA) was performed to evaluate the discrepancy in strain measurements for the three specimen configurations by using the values of the elastic modulus obtained through the three different strain measurement techniques. As such, the scientific question being addressed by this study is, if a single point strain measurement (strain gauges) is representative

of the overall structure behavior in inhomogeneous materials compared to a line strain measurement (DSS) and surface strain measurement (DIC).

Methodology

In order to answer the scientific question, experimental strain data obtained through the use of strain gauges, DSS, and DIC technique were compared for unidirectional, cross-ply, and angle-ply configuration of carbon-epoxy specimens, following the specification of the D3039 ASTM standard [1]. A preliminary comparison among the strain measurement techniques was performed through the application of the Bhattacharyya distance. The application of the Bhattacharyya method is only intended to show the closeness of the different strain measurement distributions. In order to clarify which technique provides the most accurate measurement, a B-basis analysis combined with the FEA model was necessary. Furthermore, the elastic modulus of each configuration was determined through the standard average calculation as recommended by the ASTM standard. In addition, a B-basis method was applied on the experimental data which provided a conservative value with higher confidence level in measuring the elastic modulus. Finally, the mechanical properties previously obtained were used as input in the FEA model using the commercial software Ansys Workbench^{TM}. Numerical strain data were obtained for each specimen configuration through a laminae analysis and a lamina-lamina analysis and compared to the experimental strain data. The authors also provided an overview on the three strain measurement systems employed during this study, briefly reviewing the capability of the strain gauges, DSS, and DIC along with the instrumentation of each specimen.

Specimen production and configuration

All the composite laminates were manufactured through hand layup technique at the Holistic Structural Integrity Process (HolSIP) laboratory, using off-the-shelf unidirectional carbon-epoxy prepreg DA 4518U produced by Adhesive Prepregs Composite Manufacturers (APCM) [25]. The mechanical property characterizations were performed on three different laminate configurations: unidirectional, cross-ply, and angle-ply. The corresponding layup sequence of each of the configuration are shown in Table 1 for both longitudinal and transverse pull test. The laminates were waterjet cut at Clarkson University, in which 5 specimens per test were obtained, for a total of 30 specimens. The length, the width, and the thickness varied depending on the configuration and the type of test as shown in Table 2. The specimen dimensions were in accordance to the ASTM D3039/D3039M *[1]* while the layup sequence was chosen arbitrarily.

Table 1. Lay-up sequence for the longitudinal and transverse pull test.

Specimen configuration	Lay-up Sequence for longitudinal pull test	Lay-up Sequence for transverse pull test
Unidirectional	$[0_3]_s$	$[90_5]_s$
Cross-ply	$[0_4, 90_2]_s$	$[90_4, 0_2]_s$
Angle-ply	$[0_3, 90, 45, -45]_s$	$[90_3, 0, -45, 45]_s$

Table 2. Recommended specimen dimensions from the ASTM standard D3039.

Fiber orientation	ASTM dimensions			Actual Dimensions		
	Length [mm]	Width [mm]	Thickness [mm]	Length [mm]	Width [mm]	Thickness [mm]
Unidirectional 0^o	250	15	1.0	250	15	0.99
Unidirectional 90^o	175	25	2.0	175	25	2.05
Cross-Ply and Angle Ply	250	25	2.5	250	25	2.35

Strain measurement systems

Tee rosettes CEA-00-125UT-350 strain gauge from VPG Micro-Measurements were employed, in which the active gauge length was 6 mm, as recommended by the D3039 ASTM standards, with a 350 Ohm resistance to minimize the heating effect due to the low-conductivity of the carbon fiber-epoxy resin material. The strain gauges were connected to a National Instrument Compact DAQ system using a C series multifunction I/O module NI-9211. The gauge factor of the longitudinal foil gauge was $2.090 \pm 0.5\%$ with a transverse sensitivity of $+0.7 \pm 0.2\%$.

In addition, an ODiSI-B DSS from LUNA Technology Inc. was employed for strain monitoring [26]. Compared to Fiber Brag Grating (FBG) in which the sensor is located at a specific section of the fiber, the DSS can interrogate thousands of points along a single commercial fiber with no gratings. The strain measurement is based on the Rayleigh backscattering principle in which the light is back-reflected due to perturbations in the optical fiber. The system captures a baseline signal under a free-strain condition. This initial baseline signal corresponds to a unique signature for that fiber section, a so called "fingerprint signal" for which any deviation from this baseline signal is directly proportional to a strain measurement (thermal or total) at that location of the fiber. The system can measure at a data acquisition rate of 23.8Hz to 250Hz depending on the fiber length of 20 m to 1 m respectively. The greater the length of the fiber sensor the lower the data acquisition rate. In addition, the system is able to capture strain at a spatial resolution of 0.65 mm to 5 mm. A $23.8\ Hz$ data acquisition rate was selected for all the tests in this study with a 50 cm fiber sensor, $1.3\ mm$ gauge length (although the system averages the strain values

every $0.65\ mm$), and a measured strain accuracy of $\pm 35\ \mu\varepsilon$ [26]. The system can operate within a strain range of $\pm 12{,}000\ \mu\varepsilon$ with a minimum and maximum temperature of $-65^{o}C$ and $300^{o}C$, respectively. For this study, polyimide fiber sensors were chosen.

Furthermore, DIC VIC-3D from Correlated Solutions was used as a non-contact 3D full field strain measurement technique [27]. The system provides in-plane and out-of-plane displacement and strains by cross-correlating blocks of pixel, known as subsets, with respect to an initial baseline which is created by capturing the free-strain condition upon clamping the specimen into the Instron Machine. The subset size is associated to the size of the speckle pattern on the surface, the camera resolution, and the selected field of view which is the distance between the camera and the specimen. Two Grasshopper cameras of 2.3 megapixel were used to capture the digital images during the entire pull test through the use of the commercial off the shelf VIC-Snap 9 software also from Correlated Solutions [27].

Specimen Instrumentations

The tests were performed in the Center for Advanced Material Processing (CAMP) laboratory at Clarkson University. An electro-mechanic testing Instron machine with a load cell of 100kN was used for all the tests. Mechanic wedge action grips of 30kN maximum force capacity were employed for all the transverse cases and the longitudinal test for the unidirectional case. Mechanic wedge action grips of 50kN maximum force capacity were employed for the longitudinal test of the cross-ply and angle-ply case due to the higher strength of the specimen configuration. Each test was performed at displacement control at a pull rate of 2mm/min and a data acquisition rate of 1Hz for all the three strain measurement systems. Ultimate Tensile Strength (UTS), Strain To Failure (STF), and Elastic modulus (E) were obtained from the corresponding stress-strain curves for each of the examined configuration. The UTS was obtained as the ratio between the maximum force before failure and the average cross-sectional area. As such, the STF parameter was determined as the strain value for the corresponding UTS point. Finally, the elastic modulus was computed by selecting the appropriate strain range of the stress-strain curve which is enclosed within the lower portion of the curve. According to the D3039 ASTM standard, the choice of this strain range is related to the STF value. For failure above $6{,}000\ \mu\varepsilon$, a strain range between $1{,}000\ \mu\varepsilon$ and $3{,}000\ \mu\varepsilon$ is recommended while failure below $6{,}000\ \mu\varepsilon$, the recommended strain range is between the 25% and 50% of the STF value.

All the tested specimens were equipped with the three strain measurement systems. Strain gauges and fiber optic were attached to the back surface of the specimen using M-bond 200 adhesive. The speckle pattern for the DIC was created using a customized roller from Correlated Solutions Inc. which provides a more homogeneous dot size distribution. The dot size was determined upon placing the camera at a specific distance (approximately 25 cm) from the specimen. Preliminary tests on a similar coupon showed that the 0.66mm dot size offered the

least noise error. The dot size and the resolution of the cameras provided a $5.3^{"}$ and $14.1^{"}$ field of view with 1624 pixels across. The DIC calibration was performed in VIC-3D v8 using a customized standard calibration target. Figure 1 shows the specimen instrumentation with the strain gauges, DSS, and DIC prior to testing. The choice of the subset size was selected in the Vic 3D software, which provided a subset size range between 29 and 33 depending on the specimen configuration that was tested. It is recommended to have a step size that is roughly a quarter of the subset size [28], which in our case was between 7 and 8. A subset size of 31 with the corresponding step size of approximately 8 provides a tracking area of 31x31 pixels for every 8 pixels. Another important aspect of the DIC system is the selection of the appropriate filter size to compute the strain values, which is given in terms of data points. For this study, the chosen filter size was 15. The product between the filter size and the step size provides the virtual strain gauge size, which in our case varied between 105 and 120 pixels. A smoothing area of 105 pixels can be converted into a physical distance by knowing the pixel size of the camera. In our case, a Grasshopper 2.3 MP camera (1920x1200 resolution) was used for all the tests with a pixel size of 5.86 µm. Therefore, the virtual strain gauge size used for this study varied between 0.6x0.6 mm and 0.7x0.7 mm.

Figure 1. Strain gauges and DSS instrumented on the back surface of the specimen (a), speckle pattern for the DIC system on the front surface of the specimen (b).

Statistical method

- Bhattacharyya distance

The statistical method based on the Bhattacharyya distance was used by the authors to obtain an initial estimate on the difference in strain measurements among the systems employed for this study. There are several statistical methods that can be used to measure the distance between two probability distributions, such as the D-statistic of Mahalanobis, the linear discriminant function, and the divergence [29] [30] [31]. However, the Bhattacharyya distance was proven to provide better results than the aforementioned methods [32] and it can be expressed as:

$$d = -\ln(\rho) \tag{1}$$

Where ρ is the Bhattacharyya coefficient:

$$\rho(p_1, p_2) = \sum_{i=1}^{N} \sqrt{p_1(x) * p_2(x) dx} \tag{2}$$

and $p_1(x)$ and $p_2(x)$ are two densities or probability of the observations *x*. In this case *x* represents the strain measurement. In other words, the Bhattacharyya distance can be expressed as the measure of the cosine of the angle between the two densities p_1 and p_2 [33]. According to the properties of the Bhattacharyya distance based on the Blackwell's theorem, if two set of parameters α and β are considered with $B(\alpha) > B(\beta)$, exists a set of prior probabilities $\pi = (\pi_1, \pi_2)$, for which:

$$P_e(\pi, \alpha) < P_e(\pi, \beta) \tag{3}$$

Where $P_e(\pi, \alpha)$ and $P_e(\pi, \beta)$ are the probability of error for the parameter set α and β, respectively. In this study, strain data along a line were compared with the Bhattacharyya method in which the set of parameters are the strain distributions obtained from the strain measurement systems. While for the DSS and DIC measurements it is possible to export a line of strain data, the strain gauge cannot be compared on a single test as it only provides a point measurement. However, the authors were able to overcome this problem by applying the Bhattacharyya distance to the five strain gauge data points obtained from the five tests of each configuration. In addition, the range of strain values analyzed through this method was chosen to be the same as the portion of the stress-strain curve used to determine the elastic modulus.

- B-basis method

The experimental strain data were processed to obtain the value of the elastic modulus for each specimen case. Therefore, each specimen configuration provided a total of five different elastic modulus values. In order to choose a reliable elastic modulus value, two statistical approaches were used: the average value recommended by the ASTM standard and the B-basis method. The A-basis and the B-basis are two statistically-based approaches required by the Metallic Materials Properties Development and Standardization (MMPDS) for choosing the appropriate design value that minimizes the failure probability of a structure due to material variability. The A-basis approach is based on the principle that at least 99% of the measured values are expected to equal or exceed the lower and upper boundaries with 95% confidence (limit on 1^{st} percentile), while the B-basis approach is based on the principle that at least 90% of the measured values are expected to be equal or exceed the lower and upper boundaries with 95% confidence (limit on 10^{th} percentile), shown in Figure 2 as T99 and T90, respectively. The S-basis is the specification minimum value which is computed as the difference between the average value and the standard deviation value reduced by a tolerance-limit factor [21].

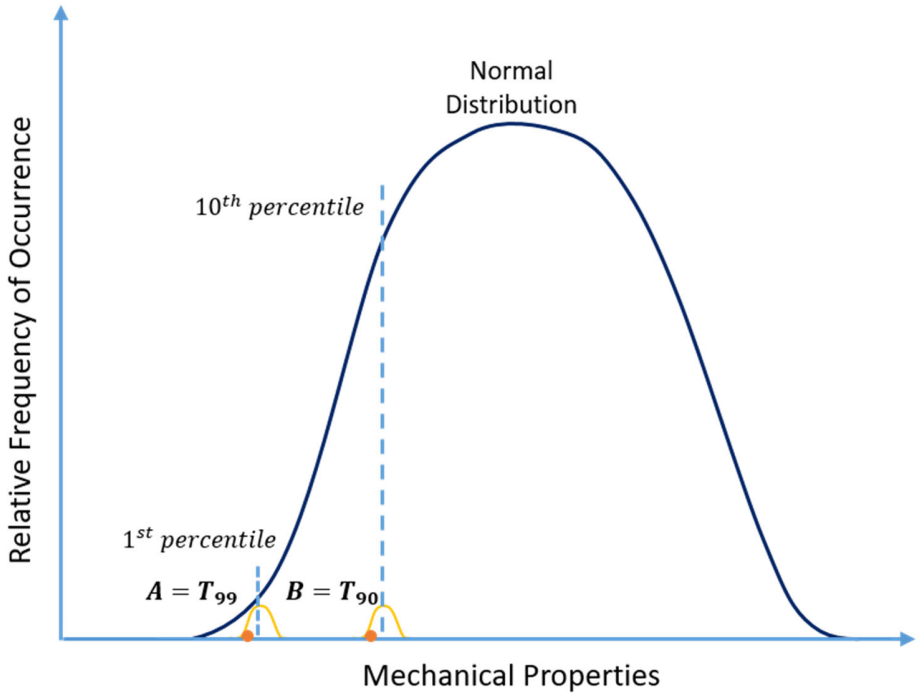

Figure 2. A-basis and B-basis specification limits

As previously mentioned, a limited number of specimens were tested for each configuration. As such, the B-basis approach is preferred to the A-basis, S-basis, and the average analysis, as it provides a more conservative value for the elastic modulus.
The B-basis values are obtained through the following equations:

$$B - basis = x_{LCB} + \frac{n}{100} * (x_{UCB} - x_{LCB}) \quad (4)$$

Where x_{LCB} and x_{UCB} are the 95% confidence lower and upper boundaries, respectively, which can be obtained from the following equations:

$$\begin{cases} x_{LCB} = \bar{x} - \frac{1.965*s}{\sqrt{n}} \\ x_{UCB} = \bar{x} + \frac{1.965*s}{\mathrm{n}} \end{cases} \quad (5)$$

Where $\bar{x}$ the sample average, s is the standard deviation, and n is the number of tested specimens.

The elastic modulus values obtained with the average and the B-basis method were used as input into the FEA model to assess the accuracy of both methods.

Finite Element Analysis methodology

A Finite Element Analysis (FEA) study was conducted through Ansys Workbench™ to ensure the validity of each of the measured elastic modulus. The authors performed two types of analysis, a laminae analysis and a lamina-lamina analysis, in which the same load, load step, boundary conditions, and mesh size were applied. In the laminae analysis the experimental elastic modulus of the overall unidirectional, cross-ply, and angle-ply laminate was used as input in the FEA model, which was modeled as one block with dimensions shown in Table 2. In the lamina-lamina analysis the experimental elastic modulus of the unidirectional 0^o and 90^o configuration was assigned for all the laminate configurations, which were created as independent layers bonded together. While in the case of the unidirectional configuration there is no differentiation between lamina and laminae since all layers are oriented in the same direction, for the cross-ply and angle-ply cases, it was necessary to define the layer orientation. Each layer was created in Ansys Composite PrepPost (ACP) using the same layup sequence of the tested specimens. A static structural analysis was performed on the solid model created in ACP upon the application of the boundary condition and the applied load, shown in Figure 3. The applied load was divided into three load steps, each of which is associated to a strain value within the range of strain used to compute the elastic modulus. An initial mesh size of 4 mm with linear elements 8-node bricks was selected for the analysis, providing 6916 nodes and 5400 elements. On a later step, a mesh convergence study with 8 mm, 6 mm, 4 mm, and 2 mm mesh size was performed. Convergence

was achieved with 4 mm mesh size, which provided percentage difference in strain measurement of 0.01% compared to the 2 mm case.

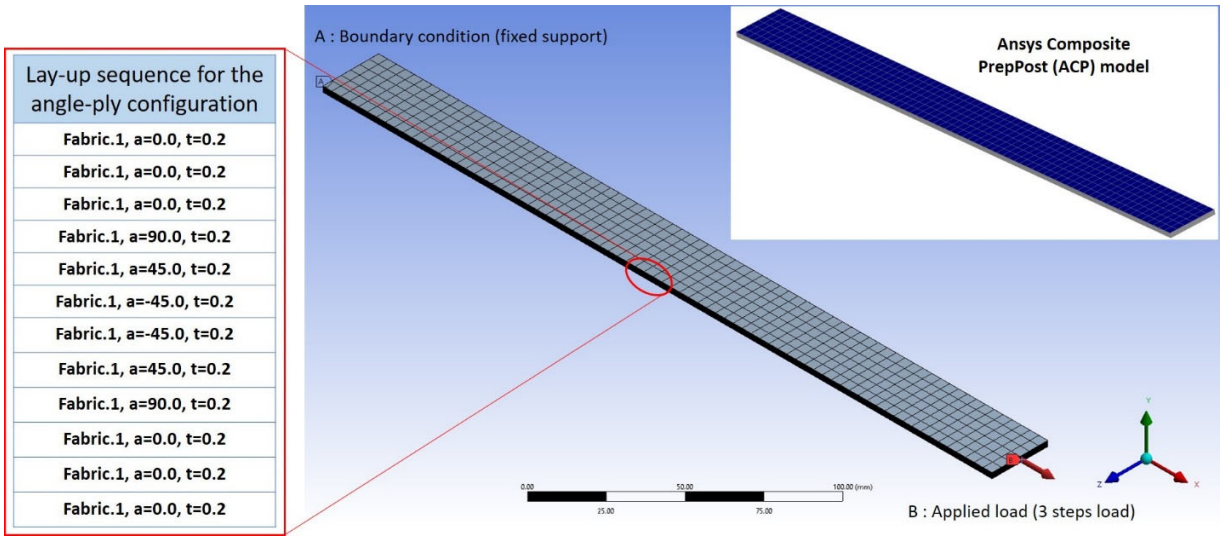

Figure 3. Mesh configuration, boundary condition and applied load.

In this study, the longitudinal and transverse elastic modulus values were determined experimentally. However, seven additional values are necessary to perform FE analysis for orthotropic or anisotropic materials such as through-thickness elastic modulus, in-plane and out-of-plane Poisson's ratio and Shear Modulus. For this reason, a parametric study was performed to assess the effect of the variation of the aforementioned properties, which were previously measured through strain gauges, following the appropriate ASTM standard [2] [3]. The material properties were increased by 50% from their original value, showing 0.01% variation in the longitudinal and transverse strain values.

Results

The following section presents the experimental data obtained from the strain gauges, DSS, and DIC system for all the specimen configurations. An uncertainty study was performed on the data set to estimate the most reliable choice among all the values obtained for the longitudinal and transverse Elastic Modulus. Finally, a Finite Element Analysis (FEA) was performed to evaluate the effect of the measurement technique on the predicted mechanical behavior of the composite material.

Experimental results

The strain values used to determine this curve were obtained as one-point evaluation (strain gauges), average of a line (DSS), and average of a surface (DIC). Five specimens were tested for each configuration. The top of Figure 4 shows the strain measured by the portion of the optical

fiber bonded on the specimen surface while the un-bonded fiber section is under a free-strain condition, as such it shows the typical strain accuracy associated with the measurement. The accuracy of the optical fiber was monitored for every sensor prior to testing. Figure 4 shows an example of the measured strain accuracy provided by the systems prior to testing, which was approximately $\pm 3\mu\varepsilon$, $\pm 25\mu\varepsilon$ and $\pm 50\mu\varepsilon$ for the strain gauges, DSS, and DIC system, respectively, which are in accordance with the minimum noise level provided by the manufacturer, as documented in [7] [26] [27]. The authors were able to lower the DSS noise down to $\pm 25\mu\varepsilon$ from the $\pm 35\mu\varepsilon$ specified in the DSS datasheet.

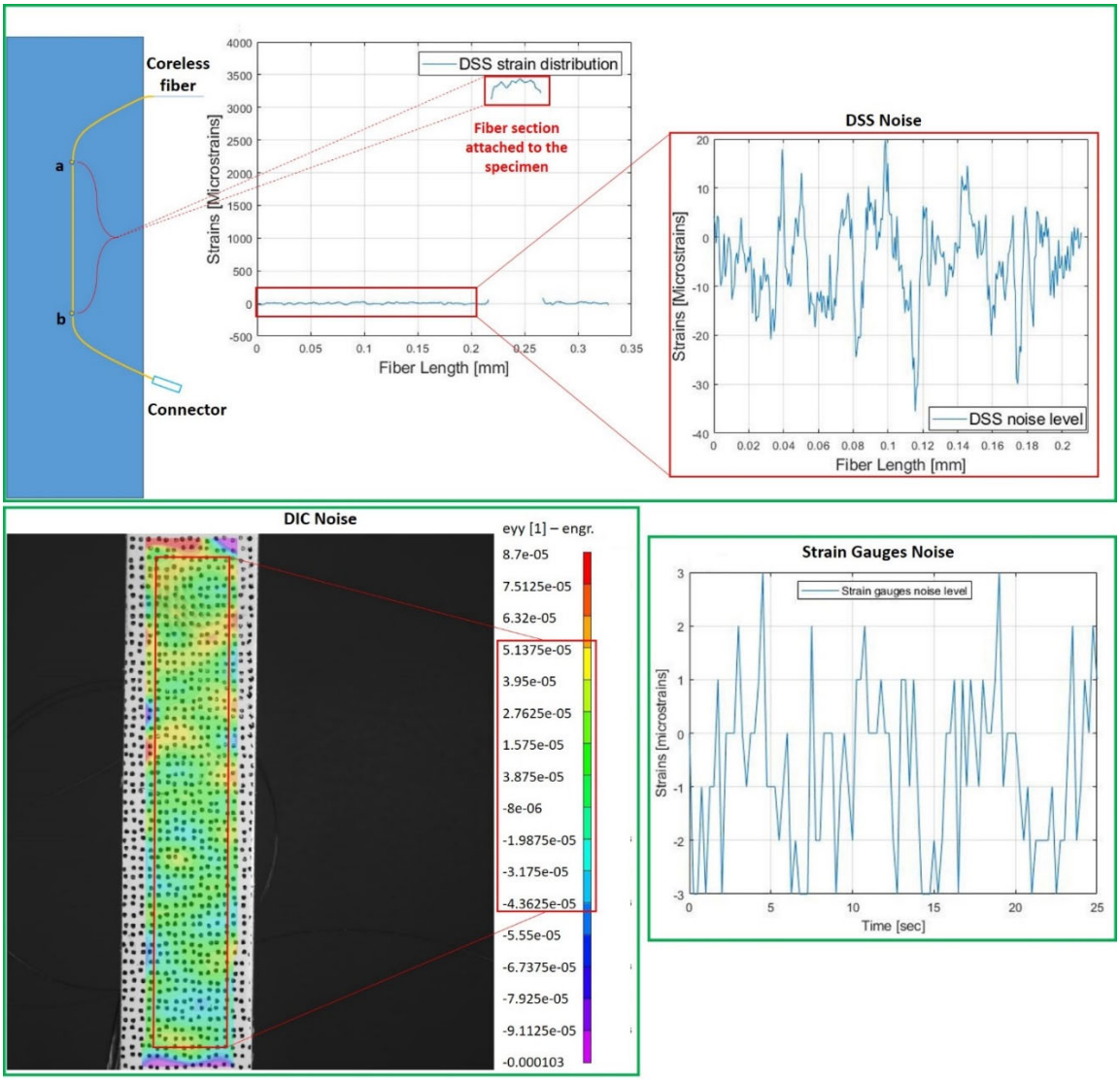

Figure 4. Noise level of the strain gauges, DSS, and DIC system.

- **Bhattacharyya distance analysis**

The Bhattacharyya distance was applied on each configuration upon performing the experimental test with the scope of providing an initial understanding of the variation on the different measured strain values. DSS and DIC strain data point along a line were evaluated and compared with the strain gauge measurement. However, due to limited space only the results of the five unidirectional E1 case were shown in Figure 5 and their combined strain data points (highlighted graph). It can be observed that the Probability Density Function (PDF) of the DSS strain data is in good agreement with the DIC strain data (with the only exception of specimen 3), while the strain gauge values, which are shown as single data point, lie within the limits of the PDF of both DSS and DIC. The authors generated a PDF from the strain gauge values to be able to adequately compare the three different techniques, shown in Figure 6. In addition, a heatmap was created on the strain gauges, DSS, and DIC strain values analyzed through the Bhattacharyya method, shown in Figure 7. The comparison between two distribution obtained from the same measurement system provides a zero distance (the two distribution are exactly the same) which is the reason of the zeros along the diagonal of each heatmap. Darker blue cells provide higher value of distance and, therefore, higher discrepancy in measured strains between two systems. The values of the Bhattacharyya distance shown in the heatmap were normalized with respect to the highest distance value, which was observed between the DSS and DIC measurement for the angle-ply E1 case providing a distance equal to 1. Overall, DSS and strain gauges seem to provide higher discrepancy while DSS and DIC seem to agree for most of the configuration.

Although a conclusion on the accuracy of each system cannot be drawn from the application of the Bhattacharyya method, it provides an initial overview on the experimental strain values.

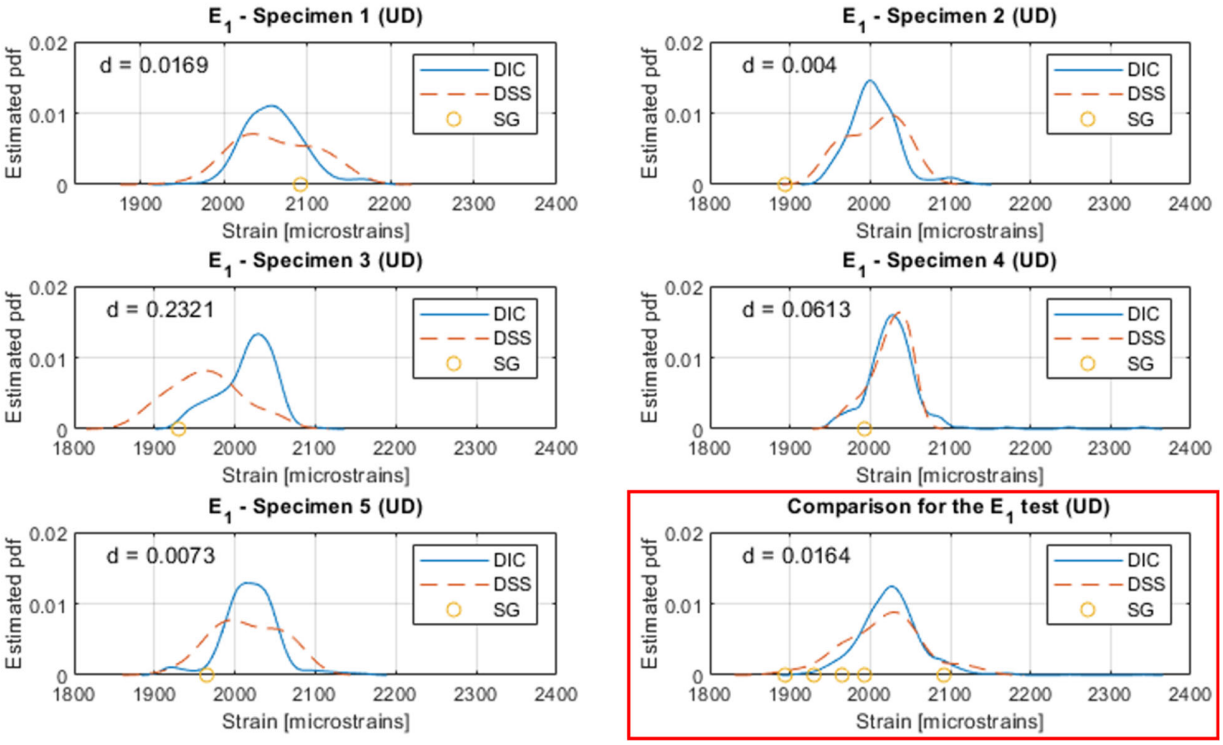

Figure 5. Bhattacharyya distance method applied on the Unidirectional E1 configuration.

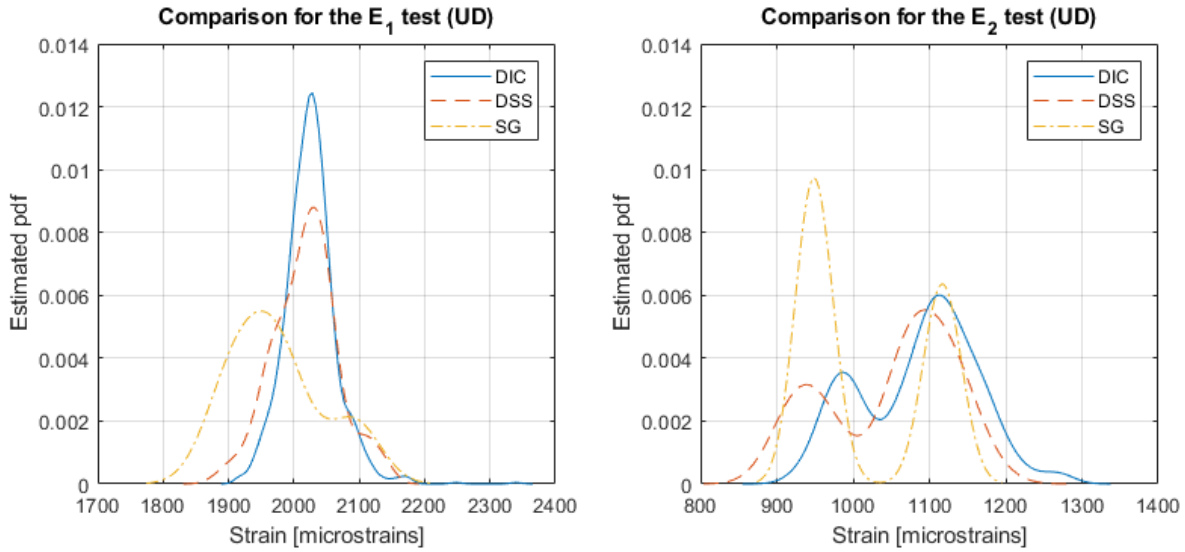

Figure 6. Probability density function of strain gauges, DSS, and DIC system for the unidirectional configuration.

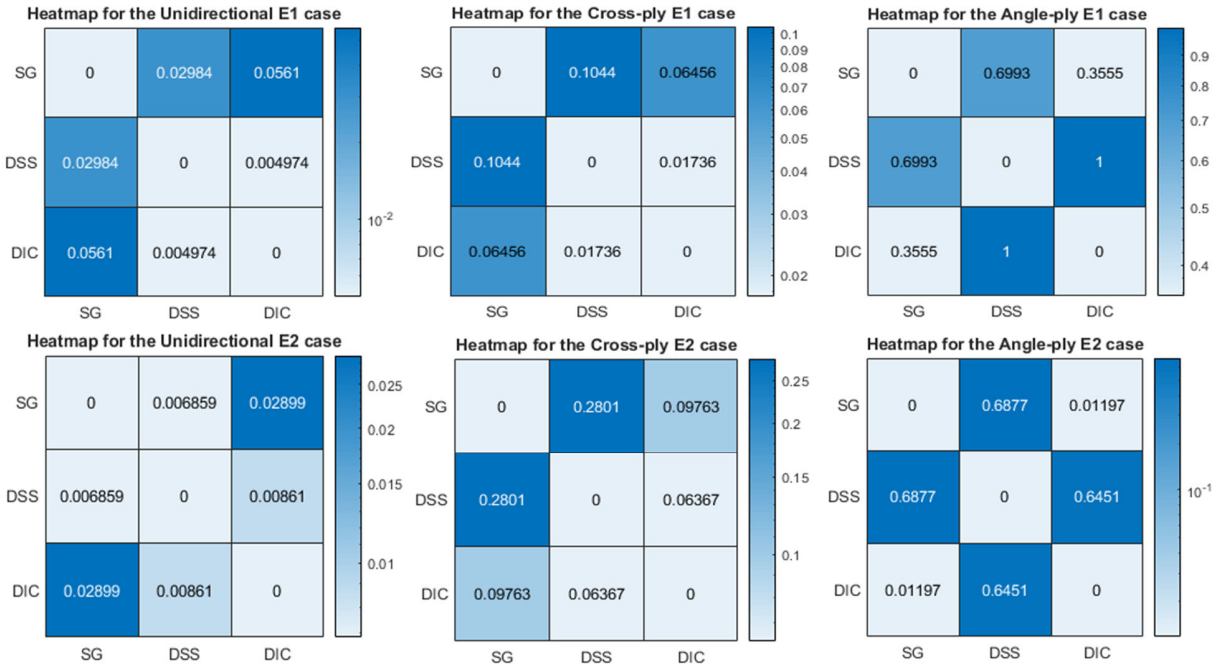

Figure 7. Heatmap for the unidirectional, cross-ply, and angle-ply configuration.

- **Unidirectional configuration**

Pull tests on the unidirectional 0^o and 90^o specimens were performed with 30kN mechanical grips. For the unidirectional 0^o case, all specimens showed a valid failure mode providing an averaged longitudinal tensile strength of approximately $1009\ MPa$ compared to the $972\ MPa$ obtained through the B-basis method. The averaged value computed for the longitudinal elastic modulus from all the tests was $105.5\ GPa$, $100.0\ GPa$, and $100.3\ GPa$ for the strain gauge, DSS, and DIC-3D, respectively while the B-basis approach provided $103.7\ GPa$, $97.6\ GPa$, and $97.9\ GPa$, respectively.

In the case of the unidirectional 90^o case, the computed averaged and B-basis strength values were approximately $17\ MPa$ and $14\ MPa$ while the computed averaged elastic modulus was $7.4\ GPa$, $7.2\ GPa$, and $7.0\ GPa$ for the strain gauge, DSS, and DIC-3D, respectively, compared to the $6.9\ GPa$, $7.0\ GPa$, and $7.0\ GPa$ obtained from the B-basis method. The averaged and B-basis STF values for both the unidirectional 0^o and 90^o case are shown in Table 3. The lower value of the B-basis analysis is due to its more conservative approach compared to the standard averaged method.

Table 3. Unidirectional Configuration for Longitudinal Elastic Modulus Determination.

Coupon	Unidirectional for E1				Unidirectional for E2			
	Strength [MPa]	Elastic modulus [GPa]			Strength [MPa]	Elastic modulus [GPa]		
		SG	DSS	DIC-3D		SG	DSS	DIC-3D
Sp1	1032	106.4	97.6	96.6	22	7.3	6.8	7.0
Sp2	1050	106.4	102.1	102.1	14	7.2	7.2	6.9
Sp3	980	102.1	96.3	97.4	20	7.6	7.4	7.1
Sp4	1040	108.2	103.5	102.9	16	6.6	8.2	6.8
Sp5	942	104.5	100.6	102.6	14	7.3	7.3	7.1
Average	**1009**	**105.5**	**100.0**	**100.3**	**17**	**7.2**	**7.4**	**7.0**
B-Basis	**972**	**103.7**	**97.6**	**97.9**	**14**	**6.9**	**7.0**	**7.0**

- **Cross-Ply configuration**

The longitudinal cross-ply configuration was tested with 50kN mechanical grips due to the expected high load to failure value. For this configuration, specimen failure was characterized by the amount of clamping pressure applied prior to testing. As such, premature failure occurred in two (specimen 2 and specimen 3) of the five specimens in proximity of the grip area which invalidated the measured strength and STF values obtained. In this case, the premature failure occurred outside the strain range used to compute the elastic modulus. This allowed the authors to determine the longitudinal elastic modulus from all the tested specimens. Strain gauge measurement for the STF value of specimen 1 was also invalid due to the disbonding of the strain gauge prior to failure. As shown in Table 4, the averaged longitudinal elastic modulus was $65.6\ GPa$, $65.2\ GPa$, and $67.7\ GPa$ for the strain gauge, DSS, and DIC-3D, respectively, compared to the B-basis values of $63.3\ GPa$, $64.3\ GPa$, and $66.9\ GPa$, respectively. The averaged longitudinal strength was approximately $850\ MPa$ while the B-basis method provided a strength value of approximately $724\ MPa$.

The transverse cross-ply configuration was tested with 30kN mechanical grips. Pull test for the transverse cross-ply configuration was characterized by two phenomena: the disbonding of the optical fiber and, as the authors of this paper denominated, a “jumping” strain measurement of the strain gauges. This was due to the fact that both strain measurement systems were attached on the specimen surface transverse to the carbon fiber direction. As such, the local failure of the 90^{o} layers created a progressive disbonding of the optical fiber. An example of the disbonding phenomenon can be observed in Figure 8, in which the strain distribution at 600 N is uniform

throughout the entire fiber section attached on the specimen surface. As the load increases to $1920\ N$, an onset of strain variation along the length of the optical fiber can be observed, although the fiber is still attached on the specimen surface. The load step of $3600\ N$ and $4723\ N$ created an onset of disbonding at the location between $170\text{-}176\ mm$ and $190\text{-}197\ mm$ of the entire fiber length. The subsequent load step of $5927\ N$ and $6829\ N$ produced a localized disbonding of the fiber, which translated into missing DSS strain data along the fiber length. For this reason, the elastic modulus was calculated within the section of the fiber in which the measured strains increased progressively with the applied load (dashed lines in Figure 8).

The same local failure of the 90^{o} layers affected the strain gauge measurements which was captured by a USB microscope, shown in Figure 9. This phenomenon generated a jumping in measured strain, as shown in Figure 10. Since this jumping effect occurred after $4000\ N$, the range of strain used to measure the elastic modulus was chosen to be between $1000\ \mu\varepsilon$ and $2000\ \mu\varepsilon$, as recommended by the D3039 ATSM standard in the case of missing or unreliable digital data. In one case (Specimen 5), the strain gauges provided an inaccurate STF value while in three cases it provided an invalid STF value (Specimen 2, 3, and 4). For the transverse cross-ply configuration, only specimen 2 failed in the proximity of the grip area and therefore it was not accounted for calculating the strength and the STF value. The averaged transverse strength was approximately $420\ MPa$ compared to the $360\ MPa$ obtained from the B-basis method. The averaged transverse elastic modulus was $32.7\ GPa$, $36.3\ GPa$, and $34.7\ GPa$ for the strain gauge, DSS, and DIC-3D, respectively, while the B-basis method showed a value of $31.9\ GPa$, $35.9\ GPa$, and $34.4\ GPa$. The experimental properties for the cross-ply configuration is shown in Table 4.

Table 4. Cross-Ply Configuration for Longitudinal Elastic Modulus Determination.

Coupon	**Cross-ply for E1**				**Cross-ply for E2**			
	Strength [MPa]	***Elastic modulus [GPa]***			***Strength [MPa]***	***Elastic modulus [GPa]***		
		SG	***DSS***	***DIC-3D***		***SG***	***DSS***	***DIC-3D***
Sp1	844	65.7	65.9	67.6	399	33.4	36.0	34.6
Sp2	729	70.0	65.5	66.3	325	31.1	37.6	34.8
Sp3	673	62.4	68.3	67.5	464	33.3	37.6	34.8
Sp4	842	66.5	66.3	68.7	421	32.4	37.9	35.2
Sp5	869	63.4	63.1	68.2	391	33.2	35.1	34.1
Average	**852**	**65.6**	**65.8**	**67.7**	**419**	**32.7**	**36.8**	**34.7**
B-Basis	**724**	**63.3**	**64.3**	**66.9**	**360**	**31.9**	**35.9**	**34.4**

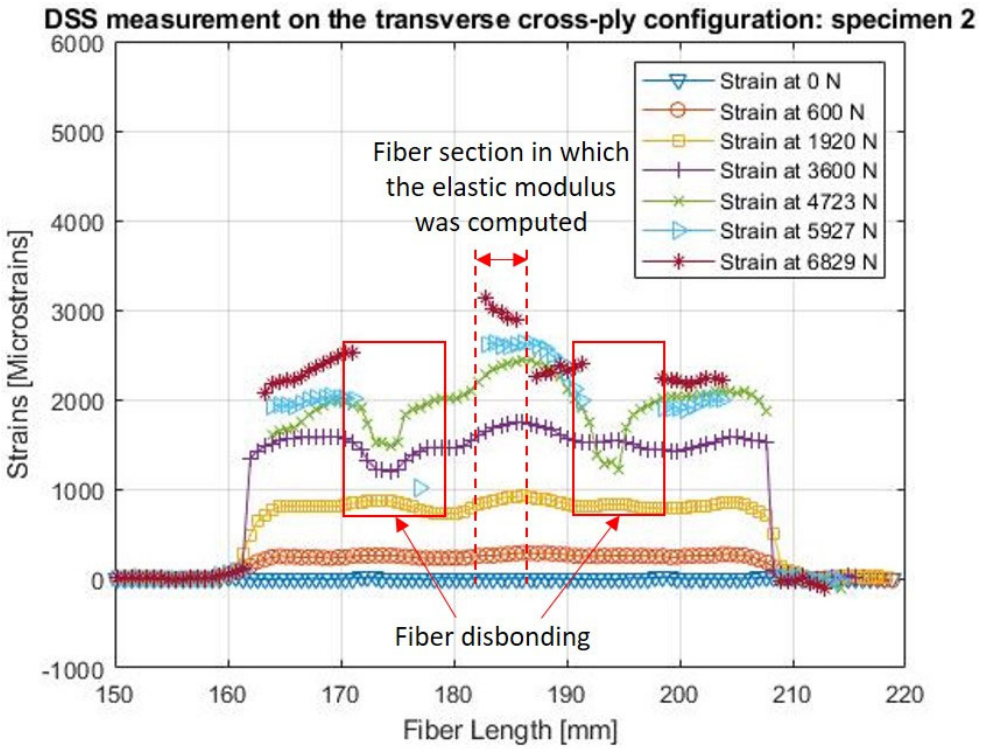

Figure 8. DSS strain measurements for specimen 2 of the transverse cross-ply configuration.

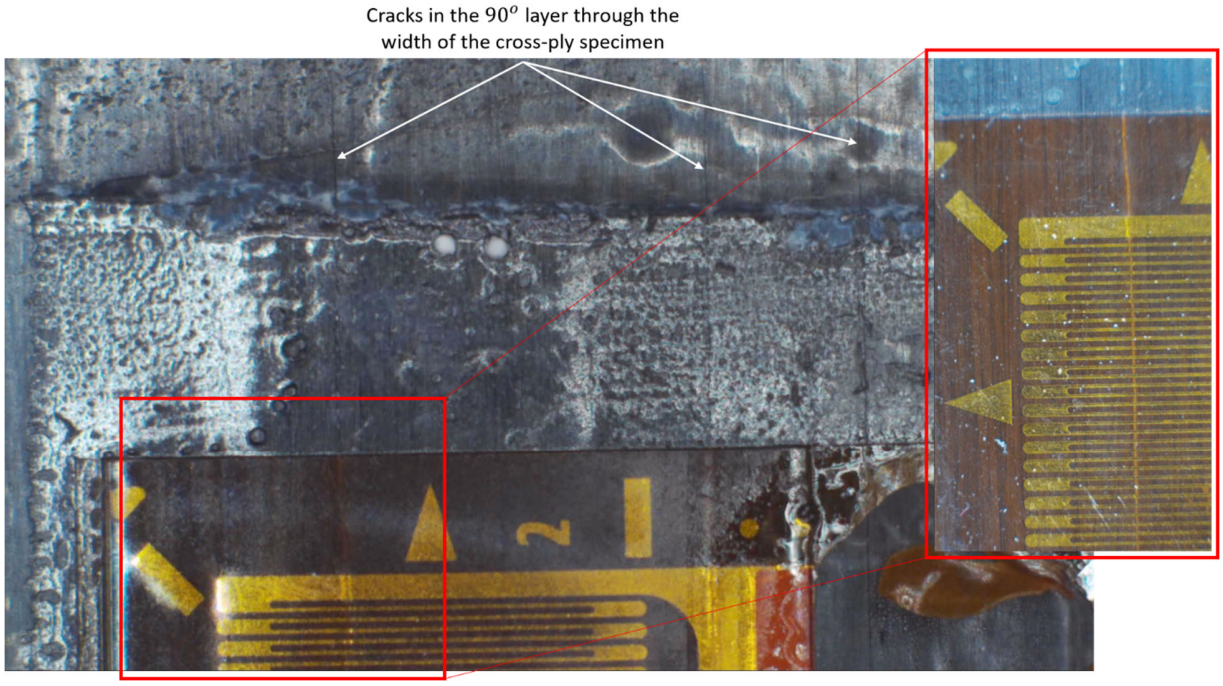

Figure 9. Local failure of the 90^o layer for the cross-ply configuration.

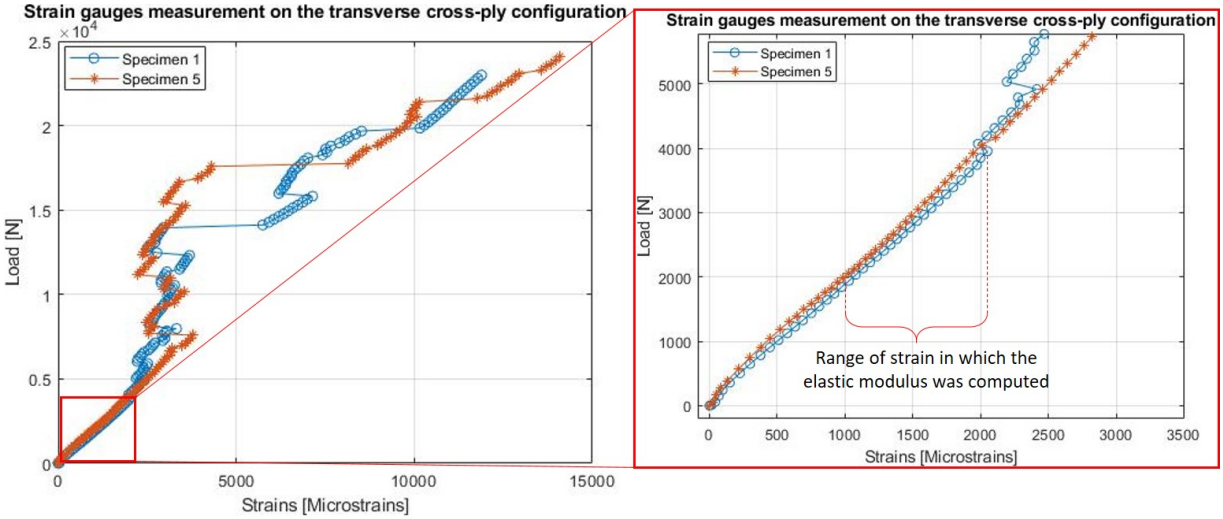

Figure 10. Strain gauge measurements for the transverse cross-ply configuration.

- **Angle-Ply configuration**

The angle-ply configuration followed the same setup as the cross-ply case in which 50kN and 30kN mechanical grips were used for the longitudinal and transverse angle-ply specimen, respectively. Strength variability on the longitudinal angle-ply configuration depends on the amount of clamping pressure applied prior to testing. Specimen 1 failed within the clamping area providing an invalid strength value, while all the remaining specimens failed within the gauge area. For this reason, the STF value of specimen 1 was not accounted for the average STF value. The averaged strength of the longitudinal cross-ply configuration was approximately $769\ MPa$ compared to the $697\ MPa$ obtained through the B-basis approach. The corresponding averaged elastic modulus was $57.1\ GPa$, $57.4\ GPa$, and $55.4\ GPa$ for the strain gauge, DSS, and DIC-3D, respectively, while the B-basis approach provided elastic modulus values of $54.9\ GPa$, $55.6\ GPa$, and $54.5\ GPa$, respectively.

The transverse angle-ply configuration was characterized by the disbonding of the optical fiber sensor with the exception of specimen 2, which partially disbonded. The range of strain used to measure the elastic modulus was chosen to be between $1000\ \mu\varepsilon$ and $2500\ \mu\varepsilon$ due to the similar jumping phenomenon shown by the strain gauges measurements as for the case of the transverse cross-ply configuration. The STF value for specimen 1 was affected by the jumping of strain prior to failure which invalidated the measurement. Failure within the clamping area for specimen 2 invalidated the measurement of the tensile strength and the STF value, which were neglected from the calculation for their corresponding average. The measured averaged and B-basis strength values were approximately $338\ MPa$ and $315\ MPa$ while the computed averaged

elastic modulus was $27.8\ GPa$, $27.6\ GPa$, and $26.8\ GPa$ for the strain gauge, DSS, and DIC-3D, respectively, compared to the $26.6\ GPa$, $25.4\ GPa$, and $26.4\ GPa$ obtained from the B-basis statistical method. Table 5 shows the averaged and B-basis of the elastic modulus and the strength values for each of the tested specimen for both the longitudinal and transverse angle-ply configuration, respectively.

Table 5. Angle-Ply Configuration for Longitudinal Elastic Modulus Determination.

Coupon	**Angle-ply for E1**				**Angle-ply for E2**			
	Strength [MPa]	***Elastic modulus [GPa]***			***Strength [MPa]***	***Elastic modulus [GPa]***		
		SG	***DSS***	***DIC-3D***		***SG***	***DSS***	***DIC-3D***
Sp1	670	59.7	56.2	56.0	336	30.1	22.9	28.1
Sp2	755	54.8	56.3	55.4	305	26.9	29.2	27.4
Sp3	737	53.5	55.1	53.4	354	26.5	29.1	26.0
Sp4	815	58.5	56.8	56.1	346	27.0	29.5	26.6
Sp5	716	59.1	56.7	56.1	316	28.8	27.4	27.3
Average	**769**	**57.1**	**56.2**	**55.4**	**338**	**27.9**	**27.6**	**27.1**
B-Basis	**697**	**54.9**	**55.6**	**54.5**	**315**	**26.6**	**25.4**	**26.4**

Finally, the readings of the strain gauges and DSS were compared to a line extraction and a point strain reading from the DIC, respectively, to assess the effect of acquiring more data samples compared to the accuracy of each technique. For brevity in this manuscript, only one specimen case for each of the six configurations is shown in Figure 11, in which the strain value corresponds to a specific load condition.

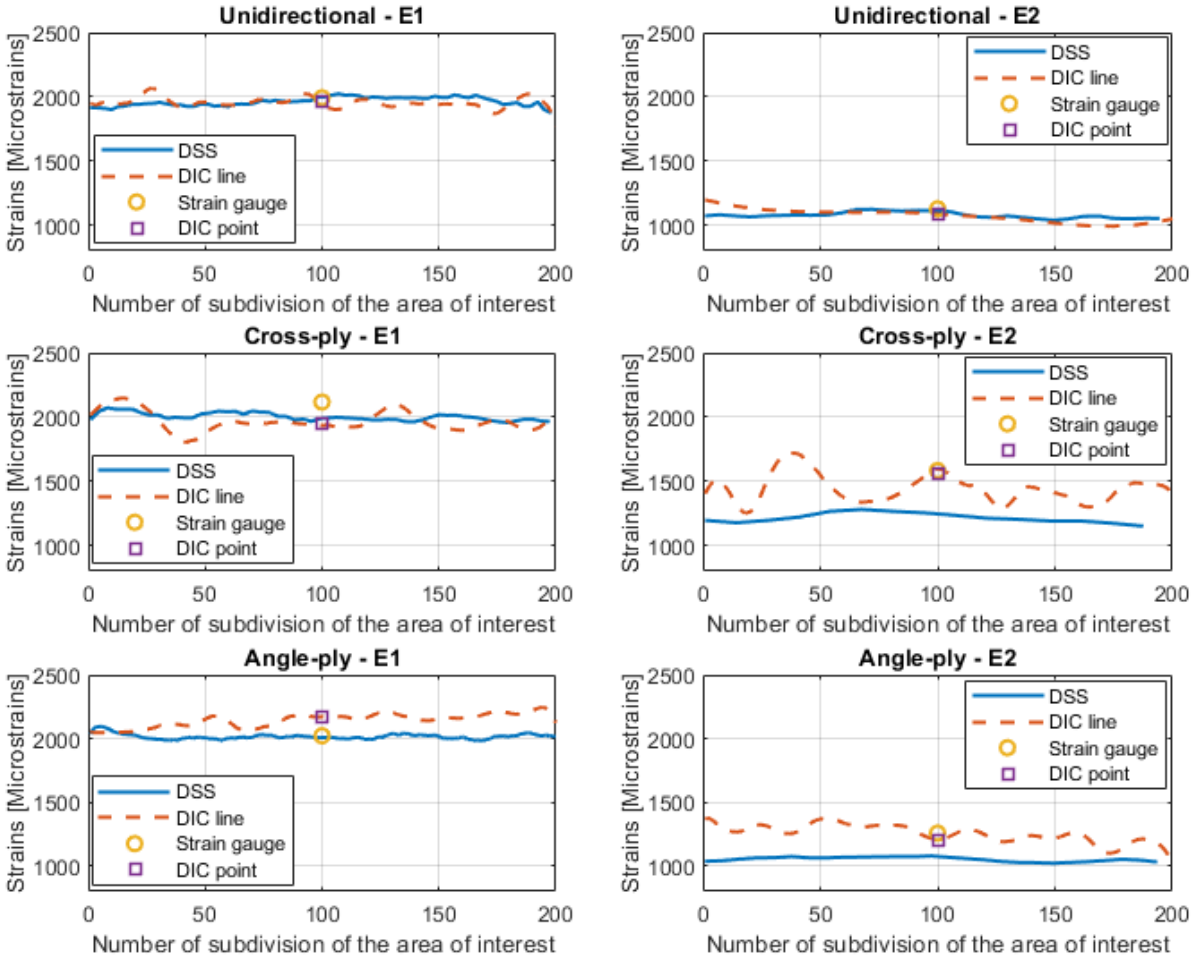

Figure 11. Strain gauge and DSS readings compared to DIC point and line extraction.

Overall, the DIC line extractions agree with the DSS measurements showing a discrepancy that is comprised within the error noise level of the DIC, with the exception of the transverse cross-ply and angle-ply case in which the DSS readings were affected by the localized disbonding of the optical fiber, as shown by the lower DSS line value compared to the DIC line extraction.

The location at which the DIC point is extracted can provide large variation in strain values. The DIC strains are computed as relative displacement of one subset cell with respect the neighboring cells and, therefore, the discrepancy between the strain gauge and the DIC point extraction becomes sensitive to the location at which the DIC point is selected. In most cases, the strain gauge values were observed to be within $150\mu\varepsilon$ compared to the DIC point extraction while only in a few cases the difference was comprised between $200\mu\varepsilon$ and $300\mu\varepsilon$.

FEA Numerical results

The measured elastic modulus was validated through a static structural analysis in Ansys Workbench™. The applied load and the experimental strain values, shown in Table 6 through

Table 17, were computed as an average from the five tested specimens for each of the configuration.

- **Unidirectional configuration**

As mentioned in the methodology section, the comparison between experimental and numerical strain was performed within a strain range between $1{,}000\ \mu\varepsilon$ and $3{,}000\ \mu\varepsilon$ (range used to compute the elastic modulus) which correspond a load range of approximately $1{,}800\ N$ and $4{,}500\ N$ for the unidirectional 0^{o} configuration. The load range value used for the analysis was obtained from the experimental stress-strain curve data as the closest available point to the range of strain values. An additional intermediate strain point at approximately $2{,}000\ \mu\varepsilon$ was used for the comparison, which correspond a load value of approximately $3{,}200\ N$. The averaged elastic modulus values, shown in Table 6, provided a maximum error of approximately 5%, 2.3%, and 0.5% for the strain gauges, DSS, and DIC-3D, respectively. The comparison performed using the B-basis method showed a maximum error of approximately 3.2%, 5.5%, and 2.9% for the strain gauges, DSS, and DIC-3D, respectively, as shown in Table 7.

Table 6. Experimental and numerical strains obtained by the averaged elastic modulus: longitudinal unidirectional case.

Averaged *E* value at lamina-lamina level: Longitudinal UD case									
Exp. Load [N]	**SG** $E_1 = 105.5\ GPa$ $E_2 = 7.4\ GPa$			**DSS** $E_1 = 100.0\ GPa$ $E_2 = 7.2\ GPa$			**DIC-3D** $E_1 = 100.3\ GPa$ $E_2 = 7.0\ GPa$		
	Exp [με]	**FEA [με]**	**Error [%]**	**Exp [με]**	**FEA [με]**	**Error [%]**	**Exp [με]**	**FEA [με]**	**Error [%]**
1816	1218	1160	5.0	1189	1224	2.9	1226	1220	0.5
3201	2109	2046	3.1	2155	2158	0.1	2149	2152	0.1
4543	2957	2905	1.8	3037	3065	0.9	3041	3055	0.5

Table 7. Experimental and numerical strains obtained by the B-basis elastic modulus: longitudinal unidirectional case.

B-basis *E* value at lamina-lamina level: Longitudinal UD case									
Exp. Load [N]	**SG** $E_1 = 103.7\ GPa$ $E_2 = 6.9\ GPa$			**DSS** $E_1 = 97.6\ GPa$ $E_2 = 7.0\ GPa$			**DIC-3D** $E_1 = 97.9\ GPa$ $E_2 = 7.0\ GPa$		
	Exp [με]	**FEA [με]**	**Error [%]**	**Exp [με]**	**FEA [με]**	**Error [%]**	**Exp [με]**	**FEA [με]**	**Error [%]**
1816	1218	1180	3.2	1189	1254	5.5	1226	1250	2.0
3201	2109	2081	1.3	2155	2211	2.6	2149	2205	2.6
4543	2957	2955	0.1	3037	3140	3.4	3041	3130	2.9

For the unidirectional 90^{o} configuration, the lower and the upper strain range value were selected as the 25% and 50% of the STF value. This percentage provided a strain value of approximately $900\ \mu\varepsilon$ and $1{,}900\ \mu\varepsilon$ for the lower and upper strain limit, respectively, which corresponds to an approximate load of $350\ N$ and $700\ N$. As such, the intermediate strain point lies at approximately $1{,}500\ \mu\varepsilon$ at an approximate load of $560\ N$. The maximum error computed by the averaged elastic modulus analysis was approximately 5%, 2.3%, and 0.5% while the B-basis analysis provided 4.4%, 2.4%, and 2.6% for the strain gauges, DSS, and DIC-3D, respectively, as shown in Table 8 and Table 9, respectively.

Table 8. Experimental and numerical strains obtained by the averaged elastic modulus: transverse unidirectional case.

Averaged *E* value at lamina-lamina level: Transverse UD case									
Exp. Load [N]	**SG** $E_1 = 105.5\ GPa$ $E_2 = 7.4\ GPa$			**DSS** $E_1 = 100.0\ GPa$ $E_2 = 7.2\ GPa$			**DIC-3D** $E_1 = 100.3\ GPa$ $E_2 = 7.0\ GPa$		
	Exp [με]	**FEA [με]**	**Error [%]**	**Exp [με]**	**FEA [με]**	**Error [%]**	**Exp [με]**	**FEA [με]**	**Error [%]**
349	902	942	4.4	935	917	2.0	944	969	2.6
557	1472	1504	2.2	1477	1464	0.9	1542	1547	0.3
705	1902	1906	0.2	1897	1853	2.4	1958	1959	0.1

Table 9. Experimental and numerical strains obtained by the B-basis elastic modulus: transverse unidirectional case.

B-basis *E* value at lamina-lamina level: Transverse UD case									
Exp. Load [N]	**SG** $E_1 = 103.7\ GPa$ $E_2 = 6.9\ GPa$			**DSS** $E_1 = 97.6\ GPa$ $E_2 = 7.0\ GPa$			**DIC-3D** $E_1 = 97.9\ GPa$ $E_2 = 7.0\ GPa$		
	Exp [με]	**FEA [με]**	**Error [%]**	**Exp [με]**	**FEA [με]**	**Error [%]**	**Exp [με]**	**FEA [με]**	**Error [%]**
349	902	983	9.0	935	969	3.6	944	969	2.6
557	1472	1570	6.7	1477	1547	4.7	1542	1547	0.3
705	1902	1987	4.5	1897	1959	3.3	1958	1959	0.1

Although the numerical analysis is in accordance to the experimental overall results due to the fact that the elastic modulus computed from the experimental stress-strain curve was used as input in the FE model, strain measured by the strain gauges showed higher strain measurement errors. A single point measurement along with the application of the more conservative B-basis method provided an even larger discrepancy between the FEA and the experimental strains gauge values, as can be seen in Table 9. Overall, the low value of error computed provided the authors with confidence on the developed FE model.

- **Cross-Ply configuration**

In case of the cross-ply configuration, the FE study was performed by using the value of the unidirectional elastic modulus for each lamina rather than the value obtained from the overall laminae. This allowed the authors to validate the previously measured unidirectional elastic modulus for both longitudinal and transverse direction. The range of strain used for the comparison are the same as the unidirectional 0^o case (i.e. between $1{,}000$ με and $3{,}000$ με). However, the corresponding range of load was comprised between approximately $4{,}000\ N$ and $12{,}000\ N$, which is higher than the unidirectional 0^o case due to the higher stiffness of the longitudinal cross-ply configuration. The comparison with the FEA model using the averaged elastic modulus value showed a maximum discrepancy of approximately 18.5%, 5.1%, and 2.7% for the strain gauges, DSS, and DIC-3D, respectively, compared to the 16.4%, 2.5%, and 0.4% values obtained from the B-basis analysis, as shown in Table 10 and Table 11, respectively.

Table 10. Experimental and numerical strains obtained by the averaged elastic modulus: longitudinal cross-ply case.

Averaged *E* value at lamina-lamina level: Longitudinal CP case									
Exp. Load [N]	**SG** $E_1 = 105.5\ GPa$ $E_2 = 7.4\ GPa$			**DSS** $E_1 = 100.0\ GPa$ $E_2 = 7.2\ GPa$			**DIC-3D** $E_1 = 100.3\ GPa$ $E_2 = 7.0\ GPa$		
	Exp [με]	**FEA [με]**	**Error [%]**	**Exp [με]**	**FEA [με]**	**Error [%]**	**Exp [με]**	**FEA [με]**	**Error [%]**
4080	1127	951	18.5	1045	1000	4.5	1025	1000	2.5
8020	2151	1871	15.0	2068	1967	5.1	2020	1966	2.7
12064	3182	2815	13.0	3107	2961	4.9	3030	2958	2.4

Table 11. Experimental and numerical strains obtained by the B-basis elastic modulus: longitudinal cross-ply case.

B-basis *E* value at lamina-lamina level: Longitudinal CP case									
Exp. Load [N]	**SG** $E_1 = 103.7\ GPa$ $E_2 = 6.9\ GPa$			**DSS** $E_1 = 97.6\ GPa$ $E_2 = 7.0\ GPa$			**DIC-3D** $E_1 = 97.9\ GPa$ $E_2 = 7.0\ GPa$		
	Exp [με]	**FEA [με]**	**Error [%]**	**Exp [με]**	**FEA [με]**	**Error [%]**	**Exp [με]**	**FEA [με]**	**Error [%]**
4080	1127	968	16.4	1045	1026	1.9	1025	1023	0.2
8020	2151	1904	13.0	2068	2018	2.5	2020	2012	0.4
12064	3182	2866	11.0	3107	3037	2.3	3030	3028	0.1

In case of the transverse cross-ply configuration, the range of strain was chosen to be between $1{,}000\ \mu\varepsilon$ and $2{,}000\ \mu\varepsilon$, which correspond a range of load of approximately $2{,}000$ N and $4{,}000$ N. Although the STF value suggested a range between $1{,}000\ \mu\varepsilon$ and $3{,}000\ \mu\varepsilon$, experimental strain gauges and DSS measurement above $2{,}000\ \mu\varepsilon$ were unreliable due to the disbonding of the fiber and the jumping strain effect shown by the strain gauges. The maximum percentage difference obtained from the averaged elastic modulus analysis was approximately 25.8%, 6.0%, *and* 9.2% for the strain gauges, DSS, and DIC-3D, respectively, as shown in Table 12. The B-basis analysis provided a maximum percentage difference of approximately 20.0%, 5.5%, *and* 4.1% for the strain gauges, DSS, and DIC-3D, respectively, as shown in Table 13.

Table 12. Experimental and numerical strains obtained by the averaged elastic modulus: transverse cross-ply case.

Averaged *E* value at lamina-lamina level: Transverse CP case									
Exp. Load [N]	SG $E_1 = 105.5\ GPa$ $E_2 = 7.4\ GPa$			DSS $E_1 = 100.0\ GPa$ $E_2 = 7.2\ GPa$			DIC-3D $E_1 = 100.3\ GPa$ $E_2 = 7.0\ GPa$		
	Exp [με]	FEA [με]	Error [%]	Exp [με]	FEA [με]	Error [%]	Exp [με]	FEA [με]	Error [%]
2082	1074	859	25.0	846	897	6.0	984	901	9.2
3034	1575	1252	25.8	1247	1307	4.8	1428	1320	8.2
3989	2014	1647	22.3	1675	1719	2.6	1881	1752	7.4

Table 13. Experimental and numerical strains obtained by the B-basis elastic modulus: transverse cross-ply case.

B-basis *E* value at lamina-lamina level: Transverse CP case									
Exp. Load [N]	SG $E_1 = 103.7\ GPa$ $E_2 = 6.9\ GPa$			DSS $E_1 = 97.6\ GPa$ $E_2 = 7.0\ GPa$			DIC-3D $E_1 = 97.9\ GPa$ $E_2 = 7.0\ GPa$		
	Exp [με]	FEA [με]	Error [%]	Exp [με]	FEA [με]	Error [%]	Exp [με]	FEA [με]	Error [%]
2082	1074	901	19.2	846	948	12.1	984	945	4.1
3034	1575	1313	20.0	1247	1382	10.8	1428	1378	3.6
3989	2014	1726	16.7	1675	1817	8.5	1881	1812	3.8

- **Angle-Ply configuration**

The angle-ply configuration followed a similar behavior to the cross-ply case. The range of strain of the longitudinal angle-ply configuration was between $1{,}000\ \mu\varepsilon$ and $3{,}000\ \mu\varepsilon$ with a corresponding load range of approximately $3{,}500$ N and $10{,}400$ N. As shown in Table 14, the maximum percentage difference provided by the averaged elastic modulus analysis was approximately 13.6%, 2.4%, and 9.2% for the strain gauges, DSS, and DIC-3D, respectively. The B-basis analysis showed a maximum percentage difference of approximately 11.7%, 2.5%, and 6.8% for the strain gauges, DSS, and DIC-3D, respectively, shown in Table 15.

Table 14. Experimental and numerical strains obtained by the averaged elastic modulus: longitudinal angle-ply case.

Averaged *E* value at lamina-lamina level: Longitudinal AP case									
Exp. Load [N]	**SG** $E_1 = 105.5\ GPa$ $E_2 = 7.4\ GPa$			**DSS** $E_1 = 100.0\ GPa$ $E_2 = 7.2\ GPa$			**DIC-3D** $E_1 = 100.3\ GPa$ $E_2 = 7.0\ GPa$		
	Exp [με]	**FEA [με]**	**Error [%]**	**Exp [με]**	**FEA [με]**	**Error [%]**	**Exp [με]**	**FEA [με]**	**Error [%]**
3561	1085	955	13.6	1023	1015	0.8	1094	1002	9.2
7037	2103	1887	11.4	2052	2007	2.2	2139	1980	8.0
10358	3063	2779	10.2	3028	2956	2.4	3122	2916	7.1

Table 15. Experimental and numerical strains obtained by the B-basis elastic modulus: longitudinal angle-ply case.

B-basis *E* value at lamina-lamina level: Longitudinal AP case									
Exp. Load [N]	**SG** $E_1 = 103.7\ GPa$ $E_2 = 6.9\ GPa$			**DSS** $E_1 = 97.6\ GPa$ $E_2 = 7.0\ GPa$			**DIC-3D** $E_1 = 97.9\ GPa$ $E_2 = 7.0\ GPa$		
	Exp [με]	**FEA [με]**	**Error [%]**	**Exp [με]**	**FEA [με]**	**Error [%]**	**Exp [με]**	**FEA [με]**	**Error [%]**
3561	1085	971	11.7	1023	1040	1.7	1094	1024	6.8
7037	2103	1920	9.5	2052	2056	0.2	2139	2025	5.6
10358	3063	2827	8.3	3028	3031	0.1	3122	2983	4.7

Strain measurements on the transverse angle-ply configuration was affected by the jumping strain effect previously mentioned for the transverse cross-ply case. Therefore, the range of strain chosen for the comparison was between approximately $1{,}000\ \mu\varepsilon$ and $2{,}000\ \mu\varepsilon$, which provided a load range of approximately $1{,}600\ N$ and $3{,}500\ N$. The computed maximum percentage difference from the averaged elastic modulus analysis was approximately 12.8%, 7.8%, and 7.9% for the strain gauges, DSS, and DIC-3D, respectively,

while the B-basis analysis provided 10.8%, 11.6%, and 5.8%, shown in Table 16 and Table 17, respectively.

Table 16. Experimental and numerical strains obtained by the averaged elastic modulus: longitudinal angle-ply case.

Averaged *E* value at lamina-lamina level: Transverse AP case									
Exp. Load [N]	**SG** $E_1 = 105.5\ GPa$ $E_2 = 7.4\ GPa$			**DSS** $E_1 = 100.0\ GPa$ $E_2 = 7.2\ GPa$			**DIC-3D** $E_1 = 100.3\ GPa$ $E_2 = 7.0\ GPa$		
	Exp [με]	**FEA [με]**	**Error [%]**	**Exp [με]**	**FEA [με]**	**Error [%]**	**Exp [με]**	**FEA [με]**	**Error [%]**
1662	1023	907	12.8	885	954	7.8	1022	947	7.9
2632	1611	1437	12.1	1456	1511	3.8	1606	1501	7.0
3527	2137	1926	11.0	1978	2026	2.4	2150	2012	6.9

Table 17. Experimental and numerical strains obtained by the B-basis elastic modulus: transverse angle-ply case.

B-basis *E* value at lamina-lamina level: Transverse AP case									
Exp. Load [N]	**SG** $E_1 = 103.7\ GPa$ $E_2 = 6.9\ GPa$			**DSS** $E_1 = 97.6\ GPa$ $E_2 = 7.0\ GPa$			**DIC-3D** $E_1 = 97.9\ GPa$ $E_2 = 7.0\ GPa$		
	Exp [με]	**FEA [με]**	**Error [%]**	Exp [με]	**Exp [με]**	**FEA [με]**	**Error [%]**	FEA [με]	**Exp [με]**
1662	1023	925	10.8	885	980	10.7	1022	966	5.8
2632	1611	1465	10.0	1456	1553	6.7	1606	1530	5.0
3527	2137	1963	8.9	1978	2081	5.2	2150	2051	4.8

Table 18 and Table 19 show a summary of the estimated percentage difference range, obtained through both averaged and B-basis method, for the lamina-lamina analysis and the laminae analysis, respectively. Although strain gauges, DSS, and DIC-3D provided different elastic modulus values, the laminae analysis shows that each system agrees with the corresponding FEA model. As such, the laminae analysis does not provide a reliable comparison between the FEA model and the estimated experimental results. The lamina-lamina analysis provides a more reliable approach as the strain values for the cross-ply and angle-ply configurations are obtained as interaction among layers using the unidirectional elastic modulus value for each layer (in case of

the lamina analysis, strain values for the cross-ply and angle-ply configurations were obtained by using the elastic modulus of those configuration).

Table 18. Summary of the estimated minimum and maximum error: averaged elastic modulus at a laminae level.

Min-Max Error [%] evaluation at laminae level							
Specimen configuration		**SG**		**DSS**		**DIC-3D**	
		Averaged	**B-basis**	**Averaged**	**B-basis**	**Averaged**	**B-basis**
UD	Longitudinal	1.8 – 5.0	0.1 – 3.2	0.1 – 2.9	2.6 – 5.5	0.1 – 0.5	2.0 – 2.9
	Transverse	0.2 –4.4	4.5 – 9.0	0.9 – 2.4	3.3 – 4.7	0.1 – 2.6	0.1 – 2.6
CP	Longitudinal	1.6 – 6.5	0.3 – 2.7	0.3 – 1.0	2.7 – 3.3	0.1 – 0.2	1.0 – 1.4
	Transverse	0.3 – 2.5	0.1 – 2.9	7.2 – 10.8	9.9 – 13.5	1.8 – 2.3	1.8 – 2.3
AP	Longitudinal	0.1 – 3.0	0.9 – 4.1	2.9 – 4.6	4.0 – 5.7	0.3 – 1.2	0.8 – 2.9
	Transverse	1.8 – 3.5	1.4 – 3.0	7.3 – 12.9	16.6 – 22.7	0.4 – 0.5	2.3 – 3.2

Table 19. Summary of the estimated minimum and maximum error: averaged elastic modulus at a lamina-lamina level.

Min-Max Error [%] evaluation at lamina-lamina level							
Specimen configuration		**SG**		**DSS**		**DIC-3D**	
		Averaged	**B-basis**	**Averaged**	**B-basis**	**Averaged**	**B-basis**
UD	Longitudinal	1.8 – 5.0	0.1 – 3.2	0.1 – 2.9	2.6 – 5.5	0.1 – 0.5	2.0 – 2.9
	Transverse	0.2 –4.4	4.5 – 9.0	0.9 – 2.4	3.3 – 4.7	0.1 – 2.6	0.1 – 2.6
CP	Longitudinal	13.0 – 18.5	11.0 – 16.4	4.5 – 5.1	1.6 – 2.9	2.4 – 2.7	0.1 – 0.4
	Transverse	22.3 – 25.8	16.7 – 20.0	2.6 – 6.0	8.5 – 12.1	7.4 – 9.2	3.6 – 4.1
AP	Longitudinal	10.2 – 13.6	8.3 – 11.7	0.8 – 2.4	0.1 – 1.7	7.1 – 9.2	4.7 – 6.8
	Transverse	11.0 – 12.8	8.9 – 10.8	2.4 – 7.8	5.2 – 10.7	6.9 – 7.9	4.8 – 5.8

Discussion

The scientific question being addressed by this study is, if the use of an average value obtained from an experimental data set using a single measurement system can be arbitrarily used in cross and angle ply configuration for the development of complex structures using the finite element method. As such, the accuracy of the strain gauges, DSS, and DIC techniques was evaluated by determining the longitudinal and transverse elastic modulus in carbon-epoxy system with unidirectional, cross-ply, and angle-ply layup sequence, performing a comparison between the experimental and numerical results. From all the collected data, it appears that the choice of a

surface strain measurements is more suitable in non-isotropic materials compared to a line or a single point measurement.

A preliminary approach to the measured experimental strain values was the application of the Bhattacharyya distance to understand the closeness of the strain distribution curve among the three different systems. Although the probability density function of the DSS and DIC was obtained through the evaluation of hundreds strain points, only five strain gauge points were available for each configuration, in addition to the fact that DIC data points were extracted along a line and not on a surface. However, the Bhattacharyya distance provided an initial overview on the measured experimental strain values in which the closeness of the strain distribution can be evaluated through the heatmap shown in Figure 7. This heat map shows that the worst-case condition occurs when comparing DSS and DIC on measuring E1 on angle-ply specimen, while the best-case condition makes use of the same two techniques (DSS and DIC) for measuring E1 on a unidirectional specimen. It is important to note that both the DSS and DIC systems make use of many points to obtain the PDF, while the strain gauge is only based on 5 data points per configuration. As such, a one to one comparison is not suitable.

All comparisons between the experimental and the numerical data were performed using the averaged values of the elastic modulus, in accordance to the ASTM standard. One of the aspect that should be considered when evaluating mechanical properties in composites is the highly data variability due to the heterogeneity of these materials, as can be seen from the strength values listed in Table 3 through Table 5. As such, the authors decided to apply the B-basis statistical method to improve the confidence in calculating the value of the elastic modulus from the experimental data. The application of the B-basis method provided more conservative elastic modulus values, which translated in higher strain obtained through the FEA. As consequence, the error values for the laminae analysis increased due to the comparison between the averaged experimental strains and the numerical strain based on the B-basis method, as shown in Table 18. Higher error bounds are obtained from the FEA lamina-lamina analysis for the cross-ply or angle ply configuration, in which the numerical strains are caused from the interaction among the layers. In this case, the B-basis method decreased the error values for the lamina-lamina analysis, providing a better estimate of the elastic modulus values, which is recommended for this type of analysis.

Some of the experimental tests on the cross-ply and angle-ply configurations were characterized by the micro-failures at an early-stage of the pull test, in which localized disbonding of the optical fiber and the “jumping effect” behavior of the strain gauge measurements were observed during test. These micro-failures are due to the high strain concentration generated at the interface between the carbon fiber and the epoxy resin in a 90^{o} layer of the composite laminate, in which the applied load is supported by the epoxy resin and not by the carbon fibers. Both disbonding

and “jumping effect” phenomena, however, did not affect the DIC-3D measurements, as such technique belongs to the category of the non-contact strain measurement systems.

The jumping effect was observed in the strain gauge measurements for the transverse cross-ply and angle-ply configuration. The outer layer of the configuration, in which the strain gauge was attached, was at 90^{o} compared to the direction of the applied load as well as the directions of the foil gauge. Each jump is associated to a local failure of the 90^{o} layer, creating a temporary change in stiffness which is restored when the applied load is supported by the inner 0^{o} layers. The jumping strain values affected the measurements at an early stage of the pull test, which made necessary a more suitable choice of strain range to calculate the elastic modulus, as recommended by the ASTM standard in case of change in slope of the stress-strain curve.

The localized disbonding of the fiber optic provides a more severe impact on the accuracy on the calculation of the elastic modulus for those configurations. The elastic modulus obtained from the DSS measurements was computed by averaging the strain values along the fiber section attached to the surface. For this reason, it was necessary to monitor the location in which the fiber progressively disbonded, in order to ignore the corresponding strain values from these section of the fiber on the average strain value calculation. This was difficult and highly time-consuming procedure since the localized disbonding happened at different points within the fiber section. In addition, in some cases the reduction in strain value at a specific location was clear and, therefore, it could be ignored from the overall average while in other cases the strain did not increase accordingly to the applied load and it was a challenge to establish whether the fiber was providing valid strain results. This created an underestimation of the strain values obtained from the DSS system for the transverse cross-ply and angle-ply cases, which lowered the error values as shown in Table 19. In support of the previous statement, Table 12 and Table 16 show experimental strain values obtained with the strain gauges and DIC-3D that are higher than the corresponding FEA strain values, with the exception of the DSS in which the FEA strain values were observed to be higher than the experimental results.

The first FEA approach to the study was performed using a laminae analysis, in which the averaged experimental elastic modulus was used as input in the FEA model. As expected, the FEA provided back numerical strain values that are similar to the experimental ones, for each system. The comparison between the experimental and the FEA results showed the higher accuracy of the DIC-3D system, as shown in Table 18, in which the error was observed to be below 1% for all the specimen configurations, with the exception of the transverse cross-ply case (the error slightly exceeded 2%). As expected, strain gauges and DSS also provided acceptable error values at the laminae level for all the configurations.

A more reliable approach chosen by the authors was the comparison between the experimental and numerical results at lamina-lamina level, in which the averaged experimental elastic modulus

of the unidirectional configuration was used as input for each layer of the FEA model (not to the entire laminate as in the previous case). This is commonly done by researchers in the engineering field due to the challenges of performing full scale tests of their finalized structures. Thus, requiring them to test the individual lamina and their material properties. However, their final results are due to the interaction of many laminas forming a full-scale structure. It was one of the objectives of this study to determine how accurate this interaction is captured by each strain measurement system and how it affects the final results in a FEA model.

The cross-ply and angle-ply configurations were modeled by changing the direction of each lamina accordingly to the corresponding lay-up sequence. For this scenario, the percentage difference was expected to be higher than the laminae analysis, as the FEA model is a perfect laminate that does not consider imperfections of any sort, such as flaws or uncertainty in the specimen cross-sectional area. Correct measurement of the unidirectional elastic modulus should provide acceptable percentage difference (within the 10% difference range) between the FEA and experimental results for each system, as observed in Table 19. These results showed that the DSS and DIC-3D data compared to the FEA results provided less than 10% difference, while the strain gauge showed a percentage difference values higher than 10% for all the non-unidirectional cases, and a 20% difference for the transverse cross-ply configuration.

Conclusion

The study demonstrated the higher accuracy of a surface strain measurements compared to a single point and a line selection measurement in non-isotropic materials. Both laminae analysis and lamina-lamina analysis showed the higher reliability of the DIC-3D system in measuring strain as compared to the strain gauges and fiber optic. In addition, the B-basis method should be used for those analysis where the experimental mechanical properties of inhomogeneous materials are used as input at a lamina level for the FEA model. Although the use of strain gauges is recommended by the ASTM standard for composite materials, this study demonstrates that the use of the DIC-3D system can provide better estimates of the mechanical parameters and thus allow for better representation of material behavior in FEA studies.

Acknowledgement

The authors kindly acknowledge the support of NVIDIA Corporation for their donation of a TESLA K40 and Quadro P6000 GPU hardware card to the Holistic Structural Integrity Process Laboratory at Clarkson University.

References

[1] ASTM International, "Standard Test Method for Tensile Properties of Polymer Matrix Composite Materials," West Conshohocken (PA), 2017.

[2] ASTM International, "Standard Test Method for Through-Thickness “Flatwise” Tensile Strength and Elastic Modulus of a Fiber-Reinforced Polymer Matrix Composite Material," West Conshohocken (PA), 2015.

[3] ASTM International, "Standard Test Method for Shear Properties of Composite Materials by the V-Notched Beam Method," West Conshohocken (PA), 2012.

[4] A. C. Manalo, T. Aravinthan and W. Karunasena, "Mechanical properties characterization of the skin and core of a novel composite sandwich structure," *Journal of Composite Materials,* vol. 47, no. 14, pp. 1785-1800, 2013.

[5] K. Baumann and J. Naumann, "Identifying the material parameters of carbon fi ber reinforced plastics with strain gages, taking transverse sensitivity into account," RAM report in applied measurement, Darmstadt, Chemnitz, 2006.

[6] A. Ajovalasit, "Advances in Strain Gauge Measurement on Composite Materials," *Strain: an International Journal for Experimetnal Mechanics,* vol. 47, pp. 313-325, 2011.

[7] V. Micro-Measurements, "Strain Gaga Measurements on Plastics and Composites," 2008.

[8] O. E. Ltd, "Strain Gauge Performance for Inhomogeneous Materials," AZO Materials, 27 09 2017. [Online]. Available: https://www.azom.com/article.aspx?ArticleID=14543. [Accessed 06 02 2019].

[9] S. S. Roberts and R. Davidson, "Mechanical Properties of Composite Materials Containing Embedded Fibre Optic Sensors," in *Fiber Optic Smart Structures and Skins IV*, 1991.

[10] J. M. SIlva, T. C. Devezas, A. P. Silva and J. A. Ferreira, "Mechanical Characterization of Composites with Embedded Optical Fibers," *Journal of Composite Materials,* vol. 39, no. 14, pp. 1261-1281, 2005.

[11] M. Surgeon and M. Wevers, "Static and dynamic testing of a quasi-isotropic composite with embedded optical fibres," *Composite Part A: Applied Science and Manufacturing,* vol. 30, pp. 317-324, 1999.

[12] M. Kashfuddoja, R. G. Prasath and M. Ramji, "Study on experimental characterization of carbon fiber reinforced polymer panel using digital image correlation: A sensitivity analysis," *OpticsandLasersinEngineering,* vol. 62, pp. 17-30, 2014.

[13] A. F. Ab Ghani and J. Mahmud, "Material Characterization of Hybrid Composite: Experimental Using Strain Gauge/DIC with Finite Element Modelling Macro/Micro Scale," *Advances on Manufacturing and Material Sciences,* vol. 740, pp. 31-40, 2017.

[14] T. He, L. Liu and A. Makeev, "Uncertainty analysis in composite material properties characterization using digital image correlation and finite element model updating," *Composite Structures,* vol. 184, pp. 337-351, 2018.

[15] M. Tekieli, S. De Santis, G. de Felice, A. Kwiecien´ and F. Roscini, "Application of Digital Image Correlation to composite reinforcements testing," *Composite Structures,* vol. 160, pp. 670-688, 2017.

[16] Y. Fukui, N. Yamanaka and Y. Enokida, "Bending strength of an Al–Al3Ni functionally graded material," *Composites Part B: Engineering,* vol. 28B, pp. 37-43, 1997.

[17] D. M. Bloyce, R. Ham-Su, K. P. Plucknett and D. S. Wilkinson, "Tape casting of SiC platelet reinforced alumina," *Advances in Ceramic–Matrix Composites: Ceramic Transactions,* vol. 38, pp. 67-78, 1993.

[18] M. J. Lamela, A. Fernandez, H. Reiter and J. Vina, "Analisis experimental y estadıstico del comportamiento a flexion dinamica de laminados de fibra de carbono y resina epoxi," Universidad Carlos III de Madrid, Madrid, 1995.

[19] W. R.C., "Statistical Distribution of Strength of Fiber-Reinforced Composite Materials," *Polymer Composite,* vol. 7, no. 2, pp. 116-123, 1986.

[20] E. Barbero, J. Fernandez-Saez and C. Navarro, "Statistical analysis of the mechanical properties of composite materials," *Composites - Part B: Engineering,* vol. 31, pp. 375-381, 2000.

[21] FAA, Metallic Materials Properties Development and Standardization (MMPDS), Columbus (OH): Battelle Memorial Institute, 2016.

[22] G. Nilakantan, A. A. Obaid, M. Keefe and J. W. Gillespie Jr, "Experimental evaluation and statistical characterization of the strength and strain energy density distribution of Kevlar KM2 yarns:

exploring length-scale and weaving effects," *Journal of composite materials,* vol. 45, no. 17, pp. 1749-1769, 2010.

[23] E. Choi and C. Lee, "Feature extraction based on the Bhattacharyya distance," *The Journal of pattern recognition society,* vol. 36, pp. 1703-1709, 2003.

[24] S. Jolad, A. Roman, M. C. Shastry, M. Gadgil and A. Basu, "A New Family of Bounded Divergence Measures and Application to Signal Detection," in *International Conference on Pattern Recognition Applications and Methods*, Lisbon, 2015.

[25] A. P. f. C. M. (APCM), "DA4518 Epoxy Prepreg System," 50 09 2018. [Online]. Available: http://www.prepregs.com/da-4518/.

[26] T. Luna Inc., "ODiSI B - Optical Distributed Sensor Interrogator," 02 02 2017. [Online]. Available: http://lunainc.com/wp-content/uploads/2016/07/ODB5_DataSheet_Rev13_020217.pdf.

[27] C. Solution, "Correlated solution: non-contacting measurement solutions," Correlated Solution, [Online]. Available: https://www.correlatedsolutions.com/. [Accessed 12 03 2019].

[28] E. Byrne, "Subset, Step Size and Strain Filter Selection," Correlated Solution, 2016.

[29] P. C. Mahalanobis, "Analysis of race mixture in Bengal," *Journal of the Anatomical Society of India,* vol. 23, pp. 301-310, 1925.

[30] R. A. Fisher, "The use of multiple measurements in taxonomic problems," *Annals of human genetics,* vol. 7, pp. 179-188, 1936.

[31] H. Jeffreys, "An invariant form for the prior probability in estimation problems," *Proceedings of the Royal Society of London, Series A, Mathematical and Physical Sciences,* vol. 186, no. 1007, pp. 453-461, 1946.

[32] T. Kailath, "THE DIVERGENCE AND BHATTACHARYYA DISTANCE MEASURES IN SIGNAL SELECTION," *IEEE transition on communication technology,* vol. 15, no. 1, pp. 52-60, 1967.

[33] A. Chattopadhyay, A. K. Chattopadhyay and C. B-Rao, "Bhattacharyya's distance measure as a precursor of genetic distance measures," *Journal of Biosciences,* vol. 29, no. 2, pp. 135-138, 2004.

[34] J. P. Hou and C. Ruiz, "Measurement of the properties of woven CFRP T300/914 at different strain rates," *Composites Science and Technology,* vol. 60, no. 15, pp. 2829-2834, 2000.

[35] Wikipedia, "Calipers," Wikipedia, [Online]. Available: https://en.wikipedia.org/wiki/Calipers. [Accessed 03 04 2019].

[36] S. R. R. J. L. A. A. S. J. L. L. Huang, "Mechanical strength of polyimide coated optical fiber at elevated temperatures," in *SPIE BIOS*, 2016.

[37] M. K. Saranath, R. Harilal, K. Mohammad and M. Ramji, "Material Characterization of Carbon Fiber Reinforced Polymer Laminate Using Virtual Fields Method," in *International Conference on Theoretical, Applied, Computational and Experimental Mechanics (ICTACEM)*, Kharagpur, India, 2014.

[38] A. F. A. Ghani, J. Mahmud and N. S. b. Muhammad, "Mechanical properties extraction of composite material using digital image correlation via open source Ncorr," *Defence S and T Technical Bulletin,* pp. 13-24, 2018.

[39] V. Munoz, M. Perrin, M.-L. Pastor, H. Welemane, A. Cantarel and M. Karama, "Determination of the elastic properties in CFRP composites:comparison of different approaches based on tensile tests and ultrasonic characterization," *Advances in Aircraft and Spacecraft Science,* vol. 2, pp. 249-260, 2015.

[40] X. Zhang, H. Hao, Y. Shi, J. Cui and X. Zhang, "Static and dynamic material properties of CFRP/epoxy laminates," *Construction and Building Materials,* vol. 114, pp. 638-649, 2016.

[41] A. international, Standard Test Method for Through-Thickness “Flatwise” Tensile Strength and Elastic Modulus of a Fiber-Reinforced Polymer Matrix Composite Material, West Conshohocken (PA): ASTM international, 2015.